Nanoscale

Accepted Manuscript

Table of contents entry

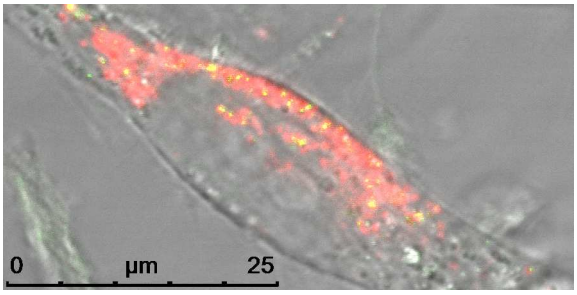

This article demonstrates the applicability of our newly developed nanodiamond-porous silica core-shell composites for concurrent cellular imaging and intracellular delivery of cargo.

Cite this: DOI: 10.1039/c0xx00000x

www.rsc.org/xxxxxx

ARTICLE TYPE

Core-shell designs of photoluminescent nanodiamonds with porous silica coatings for bioimaging and drug delivery II: Application

Neeraj Prabhakar,[a,b] Tuomas Näreoja,*[c] Eva von Haartman,[a] Didem Şen Karaman,[a] Hua Jiang,[d] Sami Koho,[c] Tatiana A. Dolenko,[e] Pekka E. Hänninen,[c] Denis I. Vlasov,[f] Victor G. Ralchenko,[f] Satoru Hosomi,[g] Igor I. Vlasov,[f] Cecilia Sahlgren[b,h] and Jessica M. Rosenholm*[a]

Received (in XXX, XXX) Xth XXXXXXXXX 20XX, Accepted Xth XXXXXXXXX 20XX
DOI: 10.1039/b000000x

Recent advances within materials science and its interdisciplinary applications in biomedicine have emphasized the potential of using a single multifunctional composite material for concurrent drug delivery and biomedical imaging. Here we present a novel composite material consisting of a photoluminescent nanodiamond (ND) core with a porous silica (SiO_2) shell. This novel multifunctional probe serves as an alternative nanomaterial to address the existing problems with delivery and subsequent tracing of the particles. Whereas the unique optical properties of ND allows for long-term live cell imaging and tracking of cellular processes, mesoporous silica nanoparticles (MSNs) have proven to be efficient drug carriers. The advantages of both ND and MSNs were hereby integrated in the new composite material, ND@MSN. The optical properties provided by the ND core rendered the nanocomposite suitable for microscopy imaging in fluorescence and reflectance mode, as well as super-resolution microscopy as a STED label; whereas the porous silica coating provided efficient intracellular delivery capacity, especially in surface-functionalized form. This study serves as a demonstration how this novel nanomaterial can be exploited for both bioimaging and drug delivery for future theranostic applications.

1. Introduction

Nanodiamonds, generally classified as diamond particles of sizes less than 100nm,[1] are members of the diverse family of nanocarbons and have recently been explored for applications in biology, medicine and imaging.[2-5] In this context, they have been found to be extremely photostable (being photoluminescent), non-toxic and exhibit good biocompatibility, making them suitable for imaging within living systems. Consequently, they have been highlighted as promising drug carriers, imaging probes, and as agents for other diagnostic and therapeutic applications.[1,2,6,7] In order to exhibit stable photoluminescence, color centers have to be produced in the ND core. The most widely used color centers for ND to be applied in bioimaging are nitrogen-vacancy (NV) centers.[8,9] These centers are active in terms of photoluminescence (PL) in neutral (NV^o) and negative (NV^-) charge states. The NV^o and NV^- are characterized by zero-phonon lines (ZPL) at 575 nm and 638 nm, respectively, which are accompanied by wide phonon bands of lower energy in PL spectra.[10] The NV luminescence can further be strongly enhanced in NDs containing large amounts of single substitutional nitrogen by irradiation of them with energetic particles (electrons, protons, helium ions).[9,11,12] Recent advances have highlighted nanodiamonds as theranostic agents combining imaging with drug delivery.[3,13] Here, the imaging modality has primarily been provided by the usage of additional fluorescent labels, whereas the drug delivery feature is accomplished by covalent[14] or adsorptive attachment[15-18] of therapeutic modalities. Although powerful, the limited surface area of the ND, tendency for aggregation and exposed nature of the therapeutic modality which might influence stability and therapeutic efficacy of the drug still render NDs far from optimal carriers.

Mesoporous silica nanoparticles (MSNs) are silica (SiO_2) nanoparticles with high porosity obtained via a supramolecular templating method. The thus attained high surface-to-volume ratio, large pore volume and tunable particle size (from <50 to >500nm) can be readily exploited for drug delivery purposes. Due to these favourable properties, the application of MSNs as potential delivery tools for controlled delivery of drugs is being vastly studied both *in vitro* and *in vivo*.[19-25] The facile surface functionalization and flexible options for modification allows for careful control of the biobehavior of the particles with the aim of achieving controlled release of drugs in targeted cells. MSNs are generally traced in the biological environment by covalent attachment of organic fluorescent dyes. Alas, as the amorphous silica matrix is rapidly biodegraded upon contact with an aqueous environment, also substantial fluorophore leakage can be expected, leading to considerable uncertainty regarding whether it is the particle itself or leached dye that is being traced.

In this study, a novel composite nanomaterial, ND@MSN, constructed by the combination of the two above-mentioned inorganic material classes, is evaluated. The novel composite is demonstrated to function as a multifunctional nanosized probe for combined bioimaging and efficient drug delivery. The applicability of the nano-based probe can be expanded by adequate surface functionalization. Coating of the ND@MSN with an organic polymer layer significantly influences the cellular uptake and prevents aggregation, especially when the aggregation is caused by the hydrophobic nature of loaded cargo. ND@MSN can be readily detected by optical means without the use of additional labels, and moreover, super-resolution imaging can be achieved with STED microscopy allowing imaging of individual particles.[26] The ND@MSN probe is proven to be safe during cellular studies. The silica coating can be biologically degraded and the ND-core is inert but safe, therefore, impressive synthetic design of the novel material can assure biocompatibility. Silica coating drastically increases the cargo carrying capability as compared to pure ND due to its porous structure, whereby the vast functionalization procedures developed for silica allow for further modification of the particle surface. This is especially critical when carrying hydrophobic cargo, which decreases the water dispersibility of the carrier, thus hampering cellular uptake. Flexible organic surface functionalization thus broadens the enormous potential of the developed inorganic/inorganic nanocomposite platform for diagnostic and therapeutic applications, as also demonstrated here.

2. Materials and Methods

2.1 Fluorescent nanodiamond production

A nanodiamond powder with meadian grain size of 50 nm produced by milling of micro-sized High Pressure - High Temperature (HPHT) diamond crystals was supplied by Tomei Diamond Co., Ltd. The nanodiamond powder was irradiated by 2 MeV electrons with a dose of 5 10^{18} cm^{-2} to create "nitrogen-vacancy" (NV) centres from single substitutional nitrogen usually presented in HPHT diamond at a level of 10^{18} cm^{-3}. After electron irradiation, the sample was annealed at 750ºC for 1 h in vacuum. The annealing allows the vacancies to migrate and attach to the nitrogen atoms in a diamond lattice, forming NV centres.[27]

2.2 Synthesis of nanodiamond-silica composite nanoparticles (ND@MSN)

2.5 mg NDs were dispersed in deionized water to a concentration of 1 mg/mL. A mixture of absoluted ethanol 2.9 mL, deionized water 4.3 mL and ammonium hydroxide solution (33%) 40 uL was prepared. The diamond dispersion was added dropwise to the water/ethanol mixture and was ultrasonicated for 30 min. A surfactant solution was made from 40 mg cetyl trimethyl ammonium bromide (CTAB) in 660 uL deionized water and 300 uL absoluted ethanol. The surfactant solution was added dropwise to the diamond suspension, which was then sonicated for another 30 min. before addition of 80uL tetraethoxy orthosilicate (TEOS). The suspension was stirred overnight at RT. The particles were separated by centrifugation at 10,000 rpm for 10 min. with acetone, extracted three times with ammonium nitrate solution (2 g/100 mL EtOH) to remove the CTAB, washed with ethanol and finally with acetone. The particles were directly redispersed to and stored as a concentration of 1 mg/mL with respect to the ND cores in acetone.

2.3 Coating of ND@MSNs with PEG-PEI copolymers (ND@MSN@cop)

Poly(ethylene glycol) – Poly(ethylene imine) (PEG-PEI) copolymers (cop) were synthesized using an in-house procedure, which will be reported elsewhere. Briefly, 1.61 g of 25kDa PEI and 2 g of HMDI (4,4′-Methylenebis(cyclohexyl isocyanate)) - activated 5kDa PEG was each dissolved in 50 mL $CHCl_3$, respectively. The PEI solution was added to the PEG solution dropwise at room temperature and subsequently the reaction flask was connected to a reflux condenser, heated up to 60 °C and reacted overnight. After the reaction, the obtained product was purified by diethyl ether and vacuum dried. ND@MSNs from an acetone suspension were washed and redispersed in HEPES (4-(2-hydroxyethyl)-1-piperazineethanesulfonic acid) buffer (pH 7.2). The copolymer was dissolved in HEPES to a concentration of 1 mg/mL and 150 wt-% (with respect to the ND) was dropwise added to the particle suspension during ultrasonication. The sample was stirred overnight at RT, washed and redispersed in HEPES. The resulting particle suspension was used for cell tests during the same day. Copolymer-coated ND@MSNs were denoted ND@MSN@cop.

2.4 Loading of active agents

ND and ND@MSN were suspended in cyclohexane. A 1 mg/mL solution of DiI (1,1′-Dioctadecyl-3,3,3′,3′-tetramethyl indocarbocyanine perchlorate) in cyclohexane was added to the suspension. The suspensions were stirred over night at RT. The particles were separated by centrifugation, washed with cyclohexane and dried in vacuum (+30°C) overnight. Copolymer coating was carried out after DiI loading for ND@MSN@cop.

2.5 Nanoparticle characterization

The produced particles were characterized by dynamic light scattering (DLS) to determine the average particle hydrodynamic size, together with zeta potential measurements (electro-kinetic potential) in HEPES buffer (25mM, pH 7.2), both conducted on a Malvern Zetasizer instrument, Model Nano ZS, Malvern, Worcestershire, UK. The instrument was equipped with a monochromatic red laser beam operating at 632.8 nm. The data was analyzed with the Malvern Dispersion Technology Software verison 6.12. For transmission electron microscopy (TEM) JEM-1200EX (Joel Ltd., Japan) samples of pure ND were dispersed in ethanol whereafter the suspended solution was transferred to electron microscopy grids and imaged. The morphology and structure of the silica coated ND@MSN was characterized by high resolution transmission electron microscopy (HRTEM) with a JEOL 2200FS (Joel Ltd., Japan) double aberration corrected FEG microscope, operating at 200kV. TEM samples were prepared by casting a drop of nanoparticle suspension onto copper grids covered with holey carbon films. Photoluminescence

(PL) spectra were recorded with LABRAM HR800 spectrometer at room temperature. The PL was excited in the samples by Argon$^+$ laser light at 488 nm wavelength. For the PL study, thin layers of ND and ND-silica particles were formed on a surface of Si substrates by drying the particles from acetone solutions. The laser beam of ~ 0.1 mW power was focused into 2 μm spots on the layers.

2.6 Sub-cellular localization and particle morphology

The following samples were prepared for the cellular TEM study: a) ND, b) ND@MSN, c) ND@MSN@cop and d) control cells (without particles). 10μg/ml concentration of each particle suspension in HEPES buffer solution (25mM, pH 7.2) was added to 100 μl cell culture. The cells were incubated for 48 h in an incubator at 37 ºC, 5% CO_2. Uranyl acetate staining was done with 1% uranyl acetate in pure water for 30 min. Lead citrate staining was done with 0.3% lead citrate in pure water for 3 min. Transmission electron microscopy of ND, ND@MSN and ND@MSN@cop nanoparticles within cells were studied with TEM microscopy. The TEM instrument was of JEM-1200EX (Jeol ltd., Japan) type. The TEM was operated at 60kV acceleration voltage.

2.7 Cellular toxicity

The toxicity of ND, ND@MSN and ND@MSN@cop nanoparticles was evaluated using WST-1 cell viability assay (Invitrogen). 10,000 HeLa cells/well were grown in a 96 well plate in DMEM (10% FCS, 1% amino acids, 1% penicillin-streptomycin) and incubated overnight. Then the growth medium was replaced by addition of a) pure NDs, b) ND@MSNs, c) ND@MSN@cop, which was prepared in HEPES buffer solution (25mM, pH 7.2). A 10ug/ml concentration (with respect to the ND mass) of particles was added into the cell media. After incubating the cells with particles for 48h, 10ul of WST-1 reagent was added to each well containing 100ul of media. The 96-well plate was incubated again for 2h at 37ºC, 5% CO_2 in an incubator. After the incubation period, the plate was read by a Varioskan Flash Multimode Reader (Thermo Scientific) to measure the absorbance at 440nm and the averaged absorbance readings were plotted. The number of viable cells was correlated with the observed absorbance from each individual sample.

2.8 Optical microscopy

a) Confocal (Leica TCS SP5 Matrix) : The experimental set up consisted of confocal microscope (Leica TCS SP5 Matrix, Leica Microsystems), LASAF (Leica application suite) software, PMT (photomultiplier tubes), photodetectors, 63X oil objectives and Argon laser 488 nm. Nanodiamonds were excited by a wavelength of 488 nm and typical emission wavelengths were 650-730 nm.

b) STED and live cell confocal (Leica TCS SP5 STED): The experimental set up consisted of confocal microscope (Leica TCS SP5 STED, Leica Microsystems), LASAF (Leica application suite) software, HyD (Hybrid GaAs-detectors), APD (Avalanche photodiode) detectors, 100X oil objectives and Argon laser 488 nm. Nanodiamonds were excited by a wavelength of 488 nm and typical emission wavelengths were 650-730 nm. In STED microscopy NDs were excited with 531nm pulse diode laser and PL was depleted with MaiTai II Ti:sapphire pulsed laser at 780 nm. Typical emission wavelengths for the STED set up were 650-730 nm.

c) Image processing for the super-resolution images was done by background subtraction and deconvolution with signal energy algorithm (LASAF). Regularisation parameters ranged from 0.25 to 0.4. For confocal deconvolution a Gaussian point spread function (PSF) with full width at half maximum (FWHM) of 230 nm was used and for STED deconvolution a Lorentzian PSF with a FWHM of 60 nm was used. When deconvolution processing was used it is indicated also in figure captions. Where no processing is indicated only brightness and contrast adjustments were made.

2.9 Live cell imaging.

A 10ug/ml concentration of particles was added into cell media. The media containing 10ug/ml of each three particles were vortexed and sonicated for 30 min. The media from 35mm culture plates was removed, washed 3X with PBS (phosphate-buffered saline solution) and 10ug/ml concentration of particles in 3ml media was added. The cells were immediately transferred to the imaging chamber. Instrument setting: (Leica TCS SP5 STED, Leica Microsystems). 63X water objective, 5%CO_2, 37ºC, Ex. 561nm laser, Em.550-600nm, HyDGaAs-detectors.

2.10 Flow cytometry

The HeLa cells were cultured in DMEM supplemented with 10% FCS in a humidified incubator at 37°C with 5% CO_2. The amount of cargo (DiO dye, 3,3´-dioctadecyloxacarbocyanine perchlorate) uptake inside cells was analyzed by BD LSRII flow cytometer (BD Biosciences). The mean fluorescence intensity observed from HeLa cells incubated with particles (ND@MSN and ND@MSN@cop) loaded with 2.5wt% DiO dye after 72h incubation was measured. The DiO sample consisted of only free DiO dye added from an ethanolic stock solution into the media. The data was analyzed with Flowing Software (Cell Imaging Core, Turku, Finland). MS excel software was used for the statistical analysis of the results.

3. Results & Discussion

3.1 Characterization of the produced nanocomposites

Silica coating of the electron-irradiated ND was performed according to the procedure reported in part I: Fabrication. DLS measurements of the ND suspensions before and after silica coating revealed an initial average size of ND centred around 200 nm which increased to 319±3nm after silica coating (see **Supplementary Figures 1a-b**). The even distribution of the resultant DLS peak (**Supplementary Figures 1b**) suggests

homogeneous coating of individual ND cores (see **Figure 1**), also supported by TEM analysis of multiple composite particles (results not shown). The zeta potential of ND@MSN nanocomposite in HEPES buffer (pH 7.2) was negative, -23.4±0.3mV, as expected for silica surfaces. The DLS measurement graphs (see **Supplementary Figure 1**) further indicates that the silica coating promotes uniform shape and less size-variation in comparison to pure nanodiamonds, in accordance with the results in part I.

After coating of the ND@MSN nanocomposites with our in-house produced PEG-PEI copolymer by electrostatic adsorption, the average particle size increased slightly to 349±8 nm with a zeta potential of +20.6±0.15mV. Thus, the surface coating with PEG-PEI copolymer yields an overall positive charge on the composite surface. This is due to the extremely high positive charge density of PEI, which is believed to anchor strongly to the negatively charged silica surface, whereas, the PEG part is neutral and does not contribute to the particle surface charge. The acquired net positive charge is beneficial in that the presence of positive charge of particle surfaces is crucial for strong interaction with the negatively charged outer membrane of cells, which is known to result in enhanced cellular uptake.[28] High net charge, positive or negative, furthermore ensures the dispersability and colloidal stability of the nanoparticles in suspension by electrostatic stabilization. The PEG portion, on the other hand, is believed to create a "molecular cushion" which can provide the system with steric stabilization, further enhancing the colloidal stability, as well as increase the "stealth" properties to avoid opsonisation by plasma proteins.[29] Plasma protein coverage would generally result in faster recognition by the body defence mechanisms with rapid elimination as a result.

To further study the structural properties of the ND and ND@MSN, and ensure proper porous silica coating had formed on the ND cores, high-resolution transmission electron microscopy (HRTEM) was applied (see **Figure 1**).

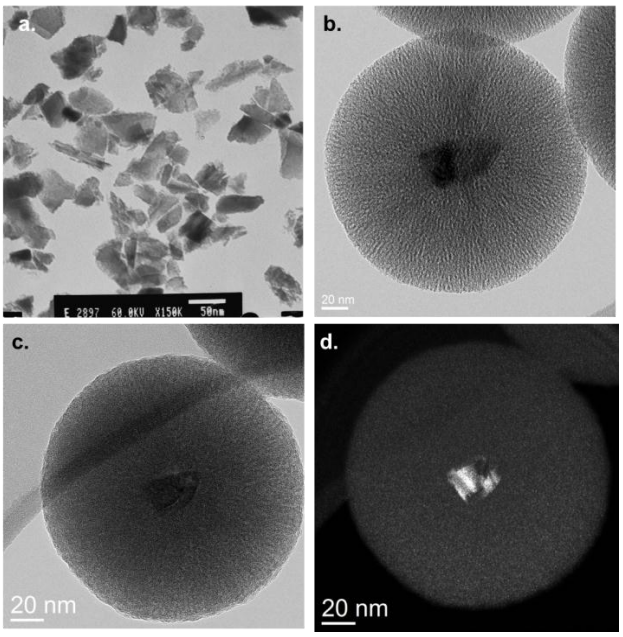

Fig.1 TEM images of ND and ND@MSN. a) Pure ND cores as imaged by TEM b) individual ND@MSN imaged by high-resolution TEM (HRTEM). Corresponding c) bright field and d) dark field image revealing the presence of a crystalline ND core.

As can be deduced from the TEM images, the coating with a silica layer improves the irregular and rough shape of NDs (**Figure 1a**). The morphological properties thus become more uniform upon silica coating both in size and shape, and the porous structure with radially aligned pores can clearly be distinguished (**Figure 1b**). The coating with such a highly porous silica layer furthermore enhances the drug-loading capability (see Part I) by significantly increasing the surface-to-volume ratio. Silica being an optically transparent material has no adverse effect on the photoluminescent (PL) properties of ND (see Part I as well as **Figure 2**). On the contrary, the PL intensity of nanodiamonds is even slightly enhanced in the ND@MSN sample as compared to pure ND (**Figure 2**). The PL enhancement is expected to be related to changes in functional state of the ND surface during the ND@MSN formation. These changes could decrease the number of electron traps quenching the PL of the NV centers close to the ND surface.

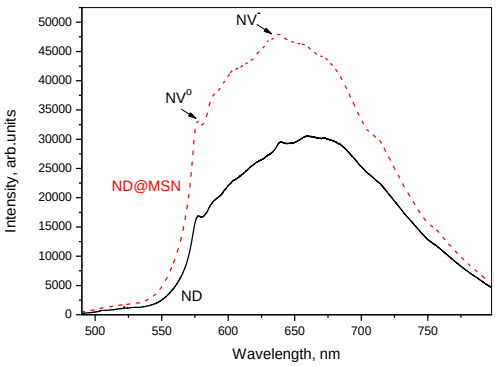

Fig. 2 PL spectra of pure ND (solid line) and ND@MSN (dashed line) recorded at 488 nm laser excitation under RT. For the PL measurements the samples were dried on a glass cover slip. Zero-phonon lines of neutral NV^o and negatively charged NV^- centers are indicated by arrows at 576 nm, and 639 nm, respectively. The spectra are normalized against the intensity of the diamond Raman peak.

3.2 Biocompatibility of the produced nanocomposites

As a prerequisite for any biomedical device, the biocompatibility should be evaluated and established for each separate modification made to the system. The biocompatibility of ND in terms of cellular viability or cytotoxicity has been previously evaluated on a range of different cell lines[30-35] and NDs have also been applied *in vivo*.[2] Amorphous silica has long been regarded as safe for drug delivery purposes[36] and silica coatings are often employed to enhance the biocompatibility of other materials.[37] However, changing the size, shape, surface roughness (e.g. porosity), surface chemistry (coating or derivatization with functional groups) or other physico-chemical properties of an inherently "safe" material may change its biobehavior, and thus the biocompatibility needs to be re-evaluated for each

modification step. Thus, the biocompatibility in terms of cell viability was evaluated using a cell culture based cytotoxicity assessment (WST-1 assay).

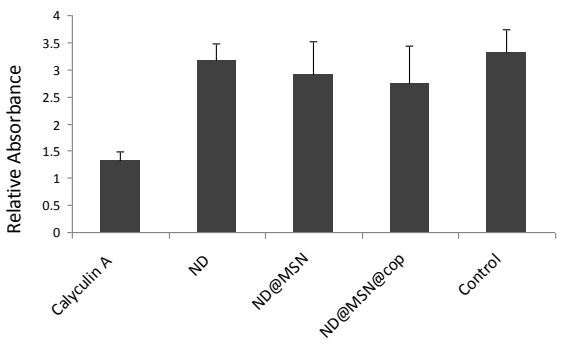

Fig. 3 Graphical representation of cell viability. The absorbance values are directly proportional to the number of viable HeLa cells. As positive control a toxin (CalyculinA 100 ng/ml) was used, whereas the negative control was untreated cells. Particles were added at a concentration of 10µg/ml with respect to the ND mass.

The cytotoxicity evaluation showed that the ND and its composites are not toxic to cells at the studied conditions (**Figure 3**). The absorbance values of the (negative) control, i.e. cells without particles, and HeLa cells incubated with ND and composites exhibit equivalent viability of cells. Both untreated and ND-treated cells remained viable after 48h incubation time, in contrast to cells treated with 100 ng/ml of the toxin Calyculin A. The viability remained very high among cells treated with all 3 different particles. Neither the addition of a silica shell nor coating of ND@MSN with PEG-PEI copolymers induced cytotoxicity. This observation is in accordance with the notation that the inert nature of diamonds and mesoporous silica has been previously individually proven safe for biological applications.[2,38,39] The cells incubated with ND@MSN@cop showed slightly lower viability but the difference was not significant. It should be noted that the concentration of nanoparticles was based on the total concentration (w/v) of nanodiamonds in all cases. Thus, in the case of the composites, the overall incubated particle mass is approximately four times that of the pure ND core sample, and the slightly lower viability observed could be due to this 4X higher total mass of the composites used in the experiment. Consequently, based on these results, coating of ND with silica and further modification with polymers seem safe to use for biomedical applications.

3.3 Optical Detectability: Particles

Confocal imaging of dried particle suspensions shows the detectability of ND@MSNs by optical microscopy (**Figure 4**). ND@MSN composite fluorescence was detectable over a range of 650-730nm. The samples were excited with a 488nm laser and reflection images of the sample can be collected over a range of 500-550nm. The reflection (backscatter) signal from ND@MSN is quite strong, and thus provides an alternate method to localize the emission signal.

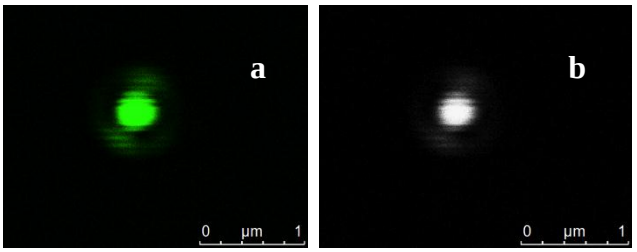

Fig. 4 Confocal microscopy images of ND@MSN. a) Reflection signal in green (Ref: 500-550nm) and b) PL-signal in grayscale (Em: 650-730nm).

Due to wide emission spectrum and superior photostability of NV centers, the NDs with NV are ideal labels for stimulated emission depletion (STED) super-resolution microscopy. A detection of isolated NV centers in type IIa CVD diamond crystal using STED technique have been demonstrated by Hell and co-workers.[26] Here we show the possibility to resolve individual luminescent NDs by STED using image processing with Lorentzian PSF (see Section 2.8). For example PL points 1 and 2 observed by conventional confocal imaging (**Fig 5a**) consist, respectively, of 3 (1', 1'' and 1''') and 2 (2' and 2'') luminescent NDs as follows from the STED imaging (**Fig 5b**). Thus STED microscopy will provide a valuable method to study and track endosome merging into late endosomes and estimate the drug load taken up by an individual cell by observing the PL signal of ND cores. The estimation can be performed even after the degradation of the MSN-copolymer – shell when ND cores have clustered together (see section 3.5). The larger diameter and surface charge of composites prevented aggregation and allowed us to resolve individual particles with standard confocal microscopy **(Supplementary Figure 2)**.

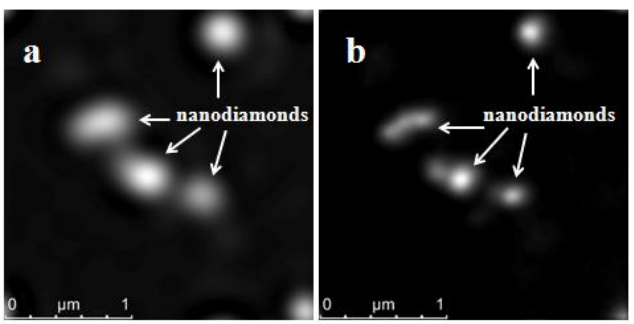

Fig. 5 Optical microscopy imaging of ND cores a) Confocal image b) STED image (Ex.531nm pulse diode laser; Em. 650-730nm; STED; 780nm). Data was processed background reduction and with signal energy based deconvolution algorithm using Gaussian PSF (FWHM 230 nm) for confocal data and Lorentzian PSF (FWHM 60 nm) for STED data.

3.4 Optical Detectability: Cells

Having established that the nanocomposite itself was optically detectable, HeLa cells were incubated with ND@MSN and ND@MSN@cop for 6h whereafter the cells were fixed to investigate the detectability in cells by confocal microscopy.

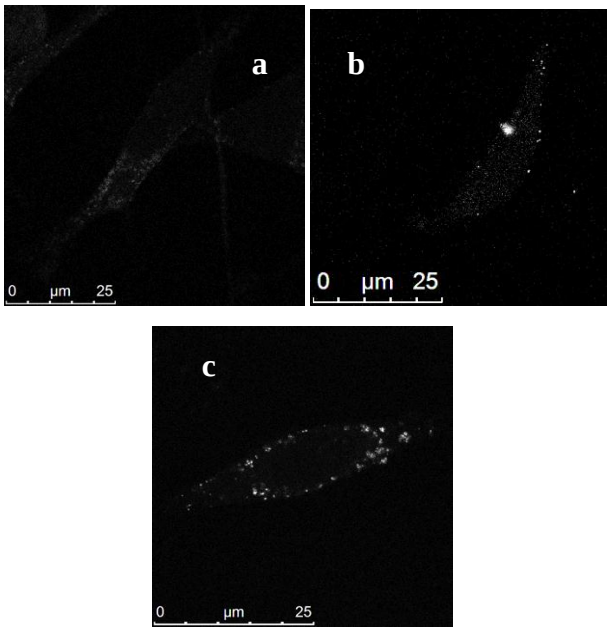

Fig.6. Photoluminescence from fixed HeLa cells incubated with a) ND, b) ND@MSN and c) ND@MSN@cop presented in greyscale. (Ex.488nm Em.650-730nm).

The emission from the ND core (650-730nm) can be clearly distinguished in the cells (**Figure 6**), indicating that both ND@MSN and ND@MSN@cop particles can be quite effectively internalized by the HeLa cells. This observation demonstrates the utility of the novel composite for certain bioimaging applications such as labelling agents for cells and intracellular tracking. As compared to the pure ND (**Figure 6a**), the emission intensity per cell is much higher (**Figure 6b-c)** and the signal is more evenly distributed throughout the cellular body. Especially the ND@MSN@cop particles (**Figure 6c)** seem to be efficiently internalized, as judged by the stronger emission signal even distribution observed. These particles seem to be mainly localized inside the cytoplasm. Large aggregates of ND@MSNs can be seen after 6h of incubation (**Figure 6b**), probably as a result of intracellular compartmentalization in endosomes. Smaller aggregates can be seen all over the cells except in the nucleus. Thus, the particles seem to be taken up by endocytosis and subsequently, especially the ND@MSN without polymer coating, form intracellular aggregates. This may be due to their inability to escape the endosomal compartment. Here, the coating of PEG-PEI copolymer serves a dual purpose: it increases the uptake and promotes endosomal escape. PEI polymers have a strong buffering ability at endosomal pH (4-6) and are thus capable of destabilizing the endosomal vesicles, causing endosomal escape.[28] Hence, the more widespread localization of ND@MSN@cop inside the cell may be an indication of the ability of this particle system to promote endosomal escape or at least prevent aggregation into multivesicular bodies. As most drugs need to reach the cytoplasm to exert their activity, such a particle system could be a potent tool for simultaneous intracellular delivery of active cargo and tracking.

3.5 Subcellular localization

Electron microscopy was employed to pinpoint the intracellular fate and localization of particles, as well as to investigate whether some intracellular trafficking route could be established.

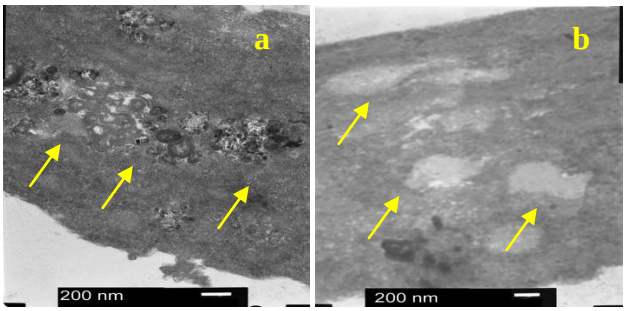

Fig.7.TEM images showing the subcellular localization of a) ND@MSN b) control cell (no particles) at 48 h.

As can be deduced from **Figure 7**, the ND@MSN composite nanoparticles are localized inside endosomal vesicles (**Fig. 7a**) whereas empty vesicles can be observed in the control cell (**Fig. 7b**).

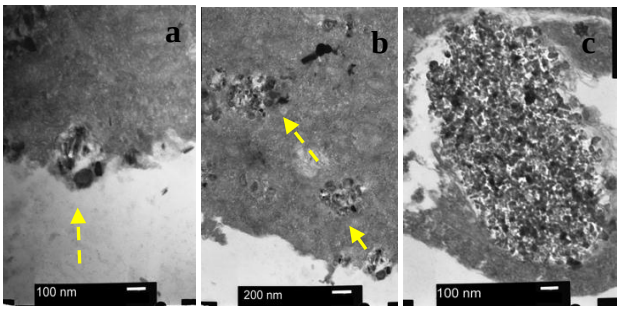

Fig. 8.ND@MSN@cop internalization route. a) TEM image of a thin section of a portion of HeLa cell showing the opening of the plasma membrane to internalize the nanodiamond composite present in the extracellular space b) Illustration of the movement of internalization and movement of ND@MSN@cop inside the cytoplasm c) large aggregation of particles inside the cell at 48 h.

After 48 h of incubation, the particles could be observed throughout the cytoplasm. Though the specific mechanism of internalization of ND@MDN@cop cannot be established based on this experiment, TEM imaging reveals the opening of the plasma membrane; and further, the particle seems to move via endosomal vesicles (**Figure 8**). The particles move across the cytoplasm and finally localize to form aggregates inside the cell's multivesicular bodies. These aggregates largely resemble that of what was observed for pure ND (see **Supplementary Figure 3**) that leads us to postulate that the coating is degraded (whereby the potential cargo would be released) within the cell, and the non-dissolvable ND cores are collected in these multivesicular bodies. This indicates that while the ND-cores are trapped in, the drug should be able to escape the endosomes for achieving effective therapeutic effect.

3.6 Intracellular delivery of loaded cargo

Having established above that cells readily internalized the composite particles, and in part I that they could further be loaded with large amounts of guest molecules, we set out to study whether this cargo could further be delivered to the cytoplasm. The chosen cargo molecule was a plasma membrane non-permeable hydrophobic, red fluorescent dye, DiI. Thus, the molecule itself does not enter cells, but stains the plasma membrane. Further, since it is a fluorescent dye, fluorescence-based techniques can be utilized to study the drug release process as well as the intracellular delivery efficiency. We have previously used this molecule as model drug to study particle-mediated intracellular delivery;[40] and thus, the efficient loading of the dye to the composite particles suggests the feasibility of these particles for similar applications. In order to avoid toxic effects due to overloading the cells with the dye and subsequent phototoxicity induced by excitation of large amounts of fluorescent dye, the particles were loaded with either 2.5 wt-% or 10wt-% DiI instead of the maximal loading determined in part I. In accordance with our previous observations, full adsorption (2.5wt%) was observed to the composites (**Figure 9**), whereas only 0.5wt% was observed to initially adsorb to the NDs when measured from the loading supernatant ("after DiI adsorption"). After separation, washing, and overnight stirring in HEPES buffer (for the pure ND to mimic the copolymer coating conditions) the amount decreased further, to 0.3 wt%. Whereas virtually no DiI leaching was observed for the ND@MSN in HEPES overnight, a slight DiI release was observed during copolymer coating under these conditions. This can be attributed to the solubilizing effect of the large excess (150wt% with respect to the ND@MSN) of added copolymer in the HEPES solution. The released DiI amount was determined by measuring the absorbance of the remaining supernatant and washing solutions. The adsorbed amount was further confirmed by elution of the dye-loaded particles into methanol and subsequent absorbance measurement of the resulting DiI-methanol eluate. The resultant HEPES suspensions (black bars, **Fig. 9**) were then further used for cellular experiments, utilizing both confocal microscopy and flow cytometry (FC).

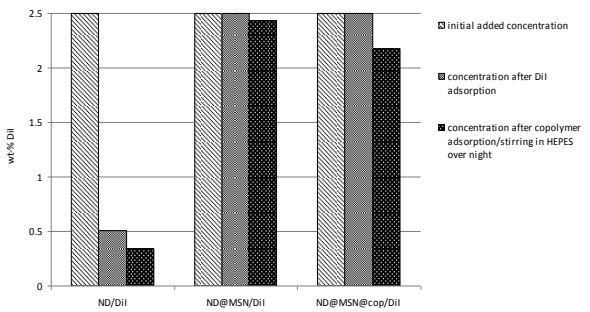

Fig. 9.Amount (wt-%) DiI dye adsorbed at different stages of the adsorption and surface modification processes.

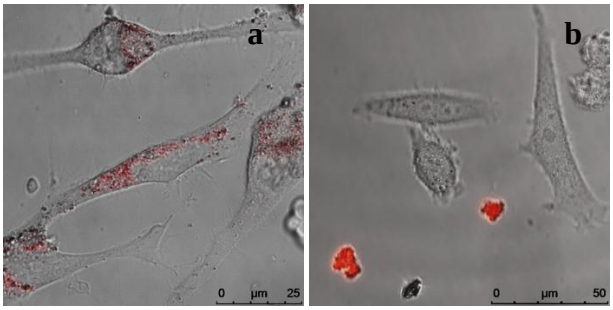

Fig. 10 Surface functionalization of nanodiamond composites facilitates the drug delivery capacity and cellular uptake. Live cell images after 24h incubation of a) Surface functionalized ND@MSN@cop nanoparticles loaded with 10wt% DiI (lipophilic membrane dye in red) and b) Uncoated ND@MSN composites loaded with 10 wt% DiI dye (in red).

Copolymer-coated ND@MSNs are designed to function as vehicles in delivering loaded cargo, e.g. drugs, to a population of cells. The polymer coating prohibits aggregation of particles, promotes cellular uptake and prevents premature release of cargo (here demonstrated with a hydrophobic dye, **Figure 10**). As the used model drug is a membrane staining agent, any dye released in the cell exterior would indeed stain only the (outer) cellular plasma membrane. The ND@MSN@cop are able to successfully permeate across the cell membrane (**Fig. 10a**), even when loaded with hydrophobic cargo. In sharp contrast, the uncoated ND@MSN loaded with hydrophobic cargo tend to form large agglomerates leading to reduced plasma membrane permeability, due to the absence of outer surface coating with a hydrophilic polymer (see **Fig. 10b**). Even though the silica coating is hydrophilic, and thus imparts the underlying ND core well-dispersed in aqueous solvent (**Supplementary information 1**) which is also seen in the cellular uptake of the composite particles (**Fig 6b**), adsorption of large amounts of hydrophobic cargo (here 10 wt-%) covers up the silica surface, resulting in an overall hydrophobic particle. On the contrary, when further coated with a hydrophilic polymer layer (PEG-PEI), this system demonstrates high cellular uptake, low particle aggregation and no premature release of cargo. This is critical since application of ND composites have a main objective of achieving drug delivery across the plasma membrane with further escape of the cargo out of the endosomal compartments. Successful intracellular delivery thus requires both high cellular uptake and release of loaded cargo into the cytoplasm. However, as the uncoated ND@MSNs become strongly hydrophobic due to effective surface coverage of hydrophobic cargo, they consequently form aggregates in aqueous environment and fail to deliver cargo across the cell membranes, thus clearly illustrating the importance of the "right" surface chemistry.

In order to quantify the delivery efficiency, live cell imaging for a selected population of cells was conducted over a release period of 72h. DiI fluorescence intensity from images acquired at 5 different time points and total intensities were analysed by ImageJ software. The DiI delivery efficiency was calculated by averaging the DiI fluorescence intensity observed during 72h (see **Fig. 11a**).

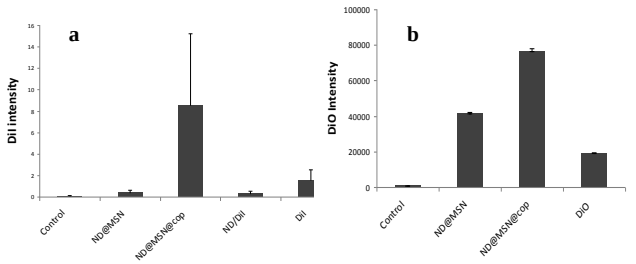

Fig.11.Quantification of the delivery efficiency mediated by nanoparticles or free dye. a) Average DiI fluorescence intensity observed microscopically from particles loaded with 2.5wt% DiI dye and incubated with HeLa cells for 72h. b) Mean DiO fluorescence intensity of DiO dye as determined by FC.

Clearly, the microscopy image analysis result (**Fig 11a**) corroborated the observations in **Figure 10** in that the copolymer coating significantly enhanced the intracellular delivery capacity. Still, the image analysis is restricted to a few cells (5 cells per time point), so to get a more quantitative result, we further studied the intracellular amount of delivered dye using flow cytometry (or FC) where 10^4 cells is considered per measurement point. To be compatible with the instrument setup (available lasers), we interchanged the dye from red fluorescent DiI to green fluorescent DiO; which is structurally similar and also used as a membrane staining (hydrophobic) dye. The mean fluorescence intensity observed from HeLa cells incubated with particles (ND@MSN and ND@MSN@cop) loaded with 2.5wt% DiO dye for 72h is illustrated in **Figure 11b**. The DiO control sample constitutes of free DiO dye (ethanol) solution added to the culture medium. Based on the FC analysis, it is shown that the PEG-PEI copolymer coating increases the cellular uptake roughly two-fold as compared to the loaded ND@MSN without polymer coating. Furthermore, the ND@MSN@cop was able to deliver a four-fold higher amount than free DiO in the medium. Some free dye "uptake" is also observed, which would also be expected as these dyes are conventionally used as plasma membrane stains, i.e. due to their hydrophobic nature they accumulate in hydrophobic parts of the cell. Here mainly to the plasma membrane, whereas dye released from ND@MSN and ND@MSN@cop avidly stains intracellular membranes as well, contributing to the higher total intensity observed. DiO fluorescence from FC for the pure ND was under the detection limit and is hence not included. The enhanced uptake in both cases (microscopy and FC) can be attributed to PEG-PEI copolymer coating providing a high positive charge density on the surface of the ND composites at physiological pH, which allows penetration across the negatively charged plasma membrane; simultaneously providing hydrophilic PEG chains improving the water dispersability of the particulate system via steric stabilization. The net positive charge on the surface of the ND composite is facilitative for permeation of the plasma membrane. Otherwise the microscopic and FC evaluations agree quite well, except in the case of the ND@MSN. The reason could be due to a lower number of cells picked for microscopy analysis, slowed down growth of cells with ND@MSN load or different nature between DiI and DiO, highlighting the fact that also the cargo properties always have to be taken into account when designing a drug delivery system.

Thus, further microscopic evaluation to investigate the intracellular model drug release process was conducted for the 2.5 wt% loaded samples (see **Figure 12**) for prolonged times in live cells.

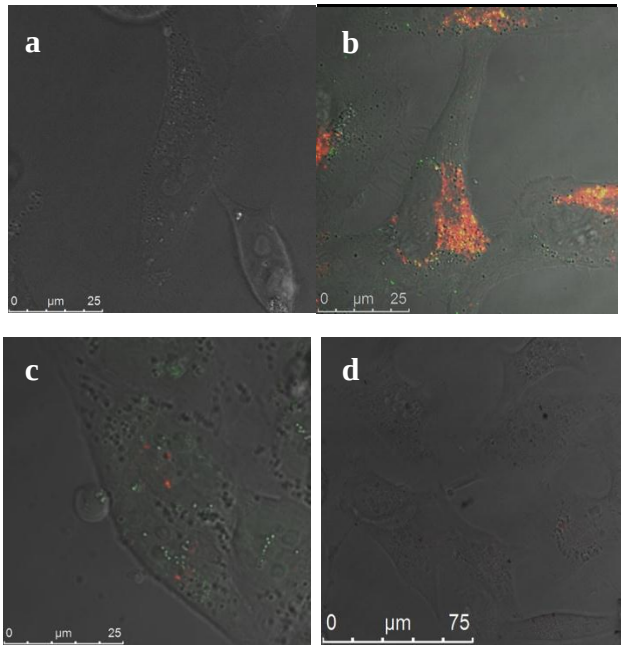

Fig.12.Microscopic evaluation of intracellular delivery efficacy by measuring DiI fluorescence after particle (loaded with 2.5wt% DiI) incubation in HeLa cells for 72hrs. a) Control cell, b) ND@MSN@cop/DiI, c) ND@MSN/DiI, and d) DiI. Red channel shows DiI emission, green/yellow a reflection from ND cores and greyscale was set to show transmission signal.

Microscopic evaluation of composite particles loaded with 2.5 wt% DiI after 72 h incubation demonstrates very high uptake as seen from abundant green/yellow ND cores and efficient intracellular release of DiI (red) for the ND@MSN@cop/DiI sample (**Fig. 12b**). Uncoated ND@MSN/DiI and cells incubated with free DiI dye solution in corresponding amounts in culture media also shows slight but significant uptake of DiI dye (**Fig. 12c&d**). As mentioned above, these lipophilic dyes are generally used as cellular stains and thus also by themselves should lead to staining of plasma membrane or a certain degree of "uptake". In order to further study the release process, special consideration was given to the ND@MSN@cop/DiI sample (**Figure 13**).

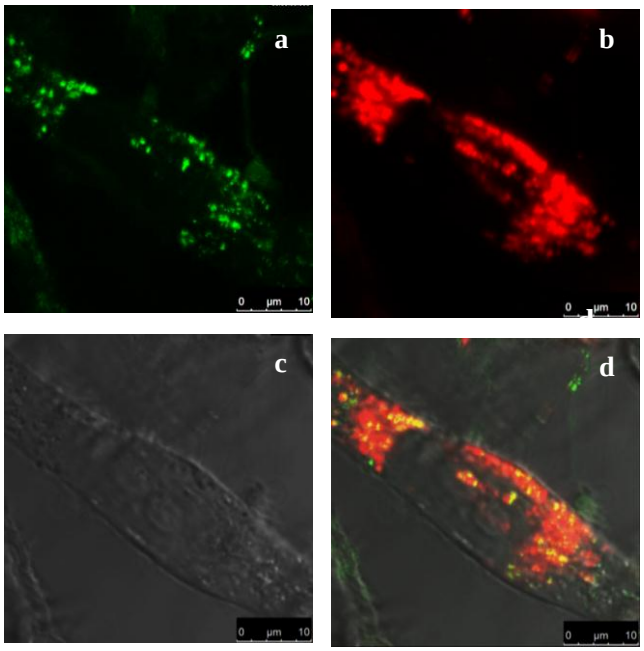

Fig. 13 Intracellular cargo release of ND@MSN@cop loaded with DiI in HeLa cells after 72h incubation. a) Reflection image (in green) showing the internalization of ND@MSN@cop particles, b) intracellular release of DiI dye (in red) from particles c) a live HeLa cell d) overlay image.

From **Fig. 13a** the reflection signal originating from the ND core can clearly be distinguished, and the intracellular pattern does not co-localize with that of the released DiI dye (**Fig 13b**). We note that this also highlights the importance of correctly distinguishing the signal originating from the particles as compared to that of added components, whereby core/shell designs are unsurpassable in this sense. Whereas the ND signal was localized to intracellular compartments, indicated by the dotted pattern, the DiI dye was seen to effectively spread throughout the cell. Thus, after 72h, the loaded cargo was very efficiently released into the cytoplasm while the particles (ND cores) remained in the endosomes (**Figure 13**). In the PEG-PEI layer, the PEI-molecules possess the ability to alter the endosomal membrane and promote cargo escape from the endosomal vesicles. This endosomal escape process is important to avoid lysosomal degradation of cargo and further for intracellular delivery to intended targets inside the e.g. cancer cells. Taken together, our data suggests that the produced ND@MSN nanocomposite could be a potent system to efficiently deliver poorly water-soluble drugs into cells, especially in surface-functionalized form.

Conclusions

Our hereby presented novel nanocomposite has been evaluated for its biomedical applicability in terms of optical detectability using biologically relevant instrumentation without the usage of labels as well as intracellular cargo delivering capacity. This novel composite, due to its ND core, is a promising candidate to overcome the shortcomings of currently used fluorescent markers. This is due to the unique nitrogen-vacancies (NV) centres (the number of which can furthermore be increased by irradiation) of NDs that emit bright internal fluorescence. Such an irradiated ND core was here coated with a porous silica layer according to the procedure described in part I, and the feasibility of this composite was studied with respect to the proposed applications. Whereas the silica coating improved the dispersability of the ND in aqueous environment with subsequent enhanced cellular uptake, further organic modification of the ND@MSN nanocomposite rendered the particle system especially suitable for intracellular delivery of poorly soluble agents. Not only did the polymer coating allow for efficient particle uptake despite the non-favourable nature of the incorporated cargo, but the cargo was further seen released into the cytoplasm whereas the carrier particles remained compartmentalized, as judged by the localization of the ND signal. This would be the ultimate scenario for a nanoparticluate drug delivery carrier, as the particles can subsequently be exocytosed from such compartments after completed delivery. However, the final fate of the remaining ND in this sense could not be derived from the presented data, and such investigations are thus currently underway.

Acknowledgments

All authors want to thank the Academy of Finland and Russian Foundation for Basic Research bilateral project "Fluorescent nanodiamond markers and nanodiamond-silica composites for biology and medicine: Efficiency and stability of photoemission versus surface chemistry" (AKA #137101, 10-03-91752-AF_a) for financial support. The authors further acknowledge funding from the Academy of Finland (projects #140193, #260599 (J.M.R.), #131034, #218062 (C.S.) #126998 (T.N. & P.H.)), Center of Excellence for Functional Materials (Finland) (D.S.K.), ISB graduate school (T.N. & P.H.), the Federal Program of the Ministry of Education and Science of Russia, grant 8398 (T.D.), Russian Ministry of Education and Science, President's grant for leading scientific schools no. 3076.2012.2 (I.V.), and from the Russian Academy of Sciences, program no. 24 (I.V.).

Notes and references

[a] *Centre for Functional Materials, Laboratory for Physical Chemistry, Department of Natural Sciences, Åbo Akademi University, 20500 Turku, Finland.. E-mail: jerosenh@abo.fi*
[b] *Turku Centre for Biotechnology, University of Turku and Åbo Akademi University, FI-20521 Turku, Finland; and Department of Biosciences, Cell biology, Åbo Akademi University, FI-20520 Turku, Finland.*
[c] *Laboratory of Biophysics, Faculty of Medicine, University of Turku, FI-20520 Turku, Finland. E-mail: tuonar@utu.fi*
[d] *Nanomicroscopy Centre, Aalto University, FI-00076 AALTO, Espoo, Finland.*
[e] *Moscow State University, 119991 Moscow, Russia.*
[f] *General Physics Institute, Russian Academy of Sciences, 119991 Moscow, Russia.*
[g] *TOMEI DIAMOND Co. Ltd., 4-5-1 Joto Oyama Tochigi, 323-0807 Japan.*
[h] *Department of Biomedical Engineering, Technical University of Eindhoven, 2612 Eindhoven, The Netherlands.*

†Electronic Supplementary Information (ESI) available: [DLS and electrokinetic measurements, optical size measurements from PL-signal of individual particles by confocal and STED microscopy, TEM image showing the subcellular localization of pure ND]. See DOI: 10.1039/b000000x/

1 V.Y. Dolmatov, Applications of Detonation Nanodiamond. *William Andrew Publ, Norwich New York.*, 2006, 477.

2 A.M. Schrand, S.A. Ciftan Hens and O.A. Shenderova, *Crit. Rev. Solid State Mater. Sci.*, 2009,**34**, 18.

3 V. Mochalin, O. Shenderova, D. Ho and Y. Gogotsi, *Nature Nanotech.*, 2012, **7**, 11.

4 D. Ho, *ACS Nano*., 2009, ***3,*** 3825.

5 L.P. McGuinness, Y. Yan, A. Stacey, D.A. Simpson, L.T. Hall, D. Maclaurin, S. Prawer, P. Mulvaney, J. Wratchup, F. Caruso, R.E. Scholten and L.C.L. Hollenberg, *Nature Nanotechnology* .,2011,**67**, 358.

6 J. Chao, E. Perevedentseva , P. Chung , K. Liu , C. Cheng , C. Chang and C. Cheng, *Biophysical Journal.*, 2007, **93,** 2199.

7 R. Lam and D. Ho, *Expert Opin Drug Deliv*., 2009, **6,** 883.

8 C. Fu, H. Lee, K. Chen, T. Lim, H. Wu , P. Lin, P. Wei, P. Tsao, H. Chang , and W. Fann, *Proceedings of the National Academy of Sciences*., 2007, **104**, 727.

9 Y. Chang, H. Lee, K. Chen, C. Chang, D. Tsai , C. Fu , T. Lim , Y. Tzeng, C. Fang , C. Han, H. Chang and W. Fann, *Nature Nanotechnology*., 2008, **3**, 288.

10 G. Davies and M.F. Hamer, *Proceedings of the Royal Society A* 1976, **348,** 285.

11 T. Wee, Y. Tzeng, C. Han, H. Chang, W. Fann , J. Hsu , Chen. K and Y. Yull, *The Journal of Physical Chemical A*, 2007, **111,** 9379.

12 I. Vlasov, V. Ralchenko, A. Khomich, S.V. Nistor, D. Schoemaker and R. Khmelnitskii, *Physica Status Solidi (a.),* 2000, **181**, 83.

13 X.W. Ma, Y.L. Zhao and X.J. Liang, *ActaPharmacol Sin.*, 2011, **32,** 543.

14 X-Q. Zhang , R. Lam , X. Xu , E. K. Chow , H.J. Kim and D. Ho, *Adv. Mater*., 2011, **23**, 4770.

15 R.A. Shimkunas, E. Robinson, R. Lam, S. Lu, X. Xu, X.Q. Zhang, H. Huang, E. Osawa and D. Ho, *Biomaterials*,. 2009, **30,** 5720.

16 J. Li, Y Zhu, W. Li, X. Zhang, Y. Peng and Q .Huang, *Biomaterials.*, 2010, **31**, 8410.

17 A.H. Smith, E.M. Robinson, X.Q. Zhang, E.K. Chow , Y. Lin, E. Osawa, J Xi and D . Ho. *Nanoscale*., 2011 **3,** 2844.

18 E. K. Chow, X.-Q. Zhang, M. Chen, R. Lam, E Robinson, H. Huang, D. Schaffer, E. Osawa, A. Goga and D. Ho, *Sci. Transl. Med..*, 2011, ***3,*** 7321.

19 S. Wu, Y. Huang and C. Mou , *Chemical Communications*, 2011,**47,** 9972.

20 J.M. Rosenholm, C. Sahlgren and M. Lindén, *Current Drug Targets.*, 2011, **12**, 1166.

21 A. Popat, S. Hartono, F .Sthar, J. Liu, S. Qiao and G. Lu , *Nanoscale.*, 2011, **3,** 2801.

22 J.M. Rosenholm, V. Mamaeva, C. Sahlgren and M. Lindén, *Nanomedicine***7.**, 2012, 111.

23 F. Tang, L. Li and D. Chen, *Advanced Materials*, 2012, **24,** 1504.

24 P .Yang, S. Gai and J. Lin,*Chemical Society Reviews.*, 2012, **41,** 3679.

25 Z. Li, J.C. Barnes, A.Bosoy, J. Fraser Stoddart and J.I. Zink, *Chem Soc Rev*, 2012, **41**, 2590.

26 E. Rittweger, K. Young Han, S. E. Irvine, C. Eggeling and S. W. Hell, *Nature Photonics.*, 2009, **3**, 144.

27 S. Lawson, G. Davies, A.T. Collins and A. Mainwood, *Journal of Physics Condensed Matter.*, 1992, **4,** L125–31 .

28 O. Boussif, H.F. Lezoualc'h, M. Zanta, M. Mergny, D. Scherman, B. Demeneix and J. Behr, *Proceedings of the National Academy of Sciences of the United States of America*, 1995,**92**, 7297.

29 C.D.Walkey and W. Chan, *Chem. Soc. Rev*., 2012, **41**, 2780.

30 S. Yu , M. Kang, H. Chang, K. Chen and Y. Yu, *Journal of American Chemical Society.*, 2005, **127,** 17604.

31 F. Treussart , V. Jacques, E. Wu, T. Gacoin, P. Grangier and J. Roch, *Physica B*, 2006**,376–377**, 926.

32 C. Cheng, E. Perevedentseva, J. Tu, P. Chung, C. Cheng, K. Liu, J. Chao, P. Chen and C. Chang, *Applied Physics Letters*, 2007, **90,** 163903.

33 J. Chao, E. Perevedentseva, P. Chung, K .Liu, C. Cheng, C .Chang and C. Cheng, *Biophysical Journal*.,2007,**93,** 2199.

34 V. Vaijayanthimala, Y. Tzeng, H. Chang and C. Li, *Nanotechnology*, 2009, **20,** 425103.

35 T. Burleson, N. Yusuf and A. Stanishevsky, *Journal of Achievements in Materials and Manufacturing Engineering*, 2009, **37,** 258.

36 C. Barbé, J. Bartlett, L. Kong, K. Finnie, H. Q. Lin, M. L. Arkin, S. Calleja. A. Bush and G. Calleja. Adv Mater., 2004, **16,** 1959.

37 R. Ghosh, R.G. Chaudhuri and S. Paria, *Chem. Rev*., 2012, **112**, 2373.

38 S. Simovic, N. Ghouchi-Eskandar, A.M. Sinn, D. Losic and C.A. Prestidge, *Curr Drug Discov Technol*,. 2011, **8,** 269.

39 K. Liu, C. Cheng, C. Chang and J. Chao, *Nanotechnology*, 2007, **18,** 325102.

40 J.M. Rosenholm, E. Peuhu, J.E. Eriksson, C. Sahlgren and M. Lindén, *Nano Letters*, 2009**, 9,** 3308.